Magnetic structures of $R_3Ag_4Sn_4$ (R = Pr,Nd) and $Nd_3Cu_4Ge_4$

2004 J. Phys.: Condens. Matter 16 7535

(http://iopscience.iop.org/0953-8984/16/41/030)

INSTITUTE OF PHYSICS PUBLISHING JOURNAL OF PHYSICS: CONDENSED MATTER

J. Phys.: Condens. Matter **16** (2004) 7535–7544 PII: S0953-8984(04)83782-2

Magnetic structures of $R_3Ag_4Sn_4$ (R = Pr, Nd) and $Nd_3Cu_4Ge_4$

E Wawrzyńska[1], J Hernández-Velasco[2], B Penc[1], A Szytuła[1] and K Tomala[1]

[1] M Smoluchowski Institute of Physics, Jagiellonian University, Reymonta 4, 30-059 Kraków, Poland
[2] BENSC, Hahn-Meitner Institut, Glienicker Straße 100, D-14109 Berlin-Wannsee, Germany

E-mail: szytula@if.uj.edu.pl

Received 23 July 2004, in final form 2 September 2004
Published 1 October 2004
Online at stacks.iop.org/JPhysCM/16/7535
doi:10.1088/0953-8984/16/41/030

Abstract

Polycrystalline samples of $R_3Ag_4Sn_4$ (R = Pr, Nd) and $Nd_3Cu_4Ge_4$ intermetallics were studied with magnetometric, x-ray and neutron diffraction methods. All of them crystallize in the orthorhombic $Gd_3Cu_4Ge_4$-type structure, in which the rare earth atoms occupy two inequivalent crystallographic positions, and order antiferromagnetically below their Néel temperatures of 12 K in the case of $Pr_3Ag_4Sn_4$, 5 K in the case of $Nd_3Ag_4Sn_4$ and 4.5 K in the case of $Nd_3Cu_4Ge_4$. All of the investigated compounds have collinear magnetic structures at low temperatures. In the case of $Pr_3Ag_4Sn_4$ an additional phase transition to a non-collinear structure is observed. The magnetic structures were studied with the support of group theoretical considerations.

1. Introduction

The $R_3Ag_4Sn_4$ (R = Pr, Nd) and $Nd_3Cu_4Ge_4$ compounds belong to the $R_3T_4X_4$ (R—a rare earth metal, T—a transition metal, X—a p-electron element) compounds, which have been intensively investigated by us recently [1–8]. All of these isostructural compounds crystallize in an orthorhombic $Gd_3Cu_4Ge_4$-type structure (space group $Immm$, no 71) [9], in which the rare earth atoms occupy two inequivalent sublattices, and order antiferromagnetically at low temperatures revealing a great variety of magnetic structures. For this reason it is interesting to systematize their magnetic properties, which is our aim. In the course of systematic research of the ternary $R_3T_4X_4$ intermetallic compounds we present results of magnetic and neutron diffraction measurements.

2. Experimental procedure

The polycrystalline samples of $R_3Ag_4Sn_4$ (R = Pr, Nd) and $Nd_3Cu_4Ge_4$, each of the total weight of about 5 g, were synthesized through the arc-melting of stoichiometric amounts of high purity elements (3N purity for R elements, and 4N for Ag, Cu, Sn and Ge) in an Ar/Zr gettered atmosphere. The reaction products were annealed at 800 °C for a week.

The samples were subsequently examined by x-ray powder diffraction (Cu Kα radiation) in order to check their purity. The peaks in the x-ray patterns of $R_3Ag_4Sn_4$ (R = Pr, Nd) and $Nd_3Cu_4Ge_4$ were indexed in the orthorhombic $Gd_3Cu_4Ge_4$-type structure. In each specimen the presence of small amounts of a few per cent of impurities was detected. In the case of the $R_3Ag_4Sn_4$ (R = Pr, Nd) samples these small impurities were identified as RAg_2 (R = Pr, Nd, respectively) and in the case of the $Nd_3Cu_4Ge_4$ sample trace amounts of NdCuGe and $NdCuGe_2$ were found.

DC magnetic measurements were made with the use of a commercial MPMS SQUID magnetometer. For each sample two types of measurements were performed: magnetic susceptibility measurement in a field of 1 kOe in the 2–300 K temperature range (from these data effective magnetic moment μ_{eff} and paramagnetic Curie temperature θ values were obtained) and magnetization measurement for fields up to 50 kOe at about 2 K (in order to get the value of the pseudo-saturated magnetic moment and the character of the magnetization curve). Since the measured samples were in the form of powder with poorly defined shapes no demagnetization effects were taken into account.

Neutron diffractograms were obtained on the E6 instrument at the BERII reactor, Hahn-Meitner Institut, Berlin. The incident neutron wavelength was 2.4463 Å and the measurement temperatures ranged between 1.5 and 20 K. The neutron diffraction data were processed with a Rietveld-type programme: FULLPROF [10].

3. Results

3.1. Crystal structure

The neutron diffraction patterns recorded at 20, 10 and 10 K for $Pr_3Ag_4Sn_4$, $Nd_3Ag_4Sn_4$ and $Nd_3Cu_4Ge_4$, respectively, as well as the x-ray patterns recorded at room temperature, confirmed that all of them crystallize in the orthorhombic structure of $Gd_3Cu_4Ge_4$ type, described by the *Immm* space group. In this structure the rare earth atoms occupy two sites: 2d ($\frac{1}{2}$, 0, $\frac{1}{2}$) and 4e (x, 0, 0); the Ag/Cu atoms are situated at the 8n (x, y, 0) positions and the Sn/Ge atoms are at the 4f (x, $\frac{1}{2}$, 0) and 4h (0, y, $\frac{1}{2}$) positions in the crystal unit cell. The determined values of the lattice parameters a, b and c as well as the positional parameters corresponding to the minimum of the reliability factor are listed in table 1.

3.2. Magnetic structure

3.2.1. $Pr_3Ag_4Sn_4$. Figure 1(a) shows the temperature dependence of the magnetic susceptibility and of the reciprocal magnetic susceptibility of $Pr_3Ag_4Sn_4$. The susceptibility reveals a jump at a temperature of 9 K, which indicates a change of magnetic ordering and the appearance of a very weak induced magnetic moment, which disappears at 12 K. Above the Néel temperature the reciprocal magnetic susceptibility satisfies the Curie–Weiss law with a paramagnetic Curie temperature of −3.7 K and an effective Pr magnetic moment equal to 3.64 μ_{B}. The magnetization curve measured at 2 K in fields up to 50 kOe, presented in figure 1(b), shows a metamagnetic transition at 27 kOe. The magnetic moment at 2 K in a

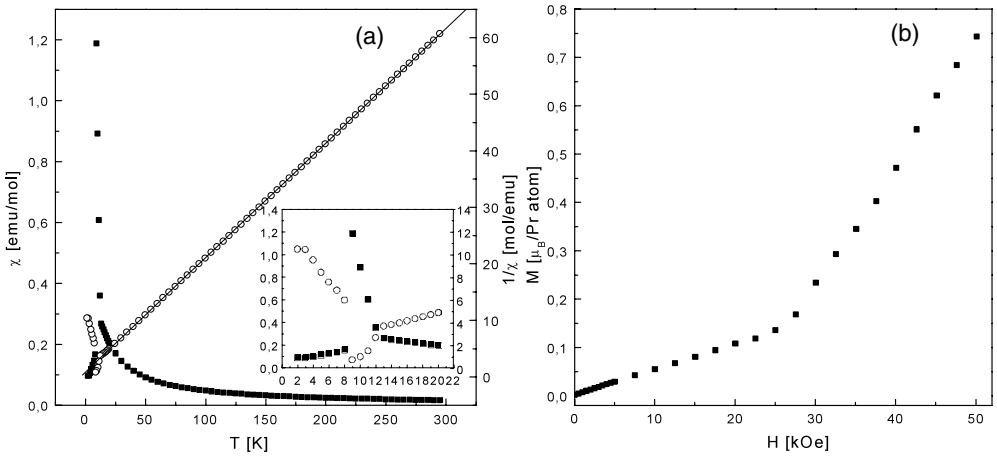

Figure 1. Temperature dependence of the magnetic susceptibility χ and the reciprocal magnetic susceptibility $1/\chi$ of $Pr_3Ag_4Sn_4$, measured at 1 kOe, and magnified 0–22 K region (part (a)) and magnetization curve measured at 2 K (part (b)).

Table 1. The refined structural and magnetic parameters of the $R_3Ag_4Sn_4$ (R = Pr, Nd) and $Nd_3Cu_4Ge_4$ compounds (space group *Immm*, no 71) obtained from the neutron diffraction data collected at different temperatures. Standard deviations are given in brackets.

	$Pr_3Ag_4Sn_4$		$Nd_3Ag_4Sn_4$		$Nd_3Cu_4Ge_4$	
T (K)	1.5	20	1.5	10	1.5	10
a (Å)	15.453(3)	15.451(4)	15.400(5)	15.404(6)	14.230(4)	14.232(5)
b (Å)	7.350(2)	7.349(2)	7.334(2)	7.339(3)	6.702(2)	6.703(2)
c (Å)	4.657(1)	4.654(1)	4.632(1)	4.632(2)	4.296(1)	4.297(1)
V (Å^3)	529.0(2)	528.5(3)	523.1(3)	523.6(3)	409.7(2)	409.9(2)
x_R	0.1343(8)	0.1393(8)	0.1306(9)	0.130(1)	0.1242(7)	0.1237(7)
$x_{Ag/Cu}$	0.3272(6)	0.3291(6)	0.3305(7)	0.3321(7)	0.3332(4)	0.3332(4)
$y_{Ag/Cu}$	0.1936(8)	0.1887(7)	0.190(2)	0.189(2)	0.189(1)	0.189(1)
$x_{Sn/Ge}$	0.2164(8)	0.2160(9)	0.211(1)	0.211(1)	0.2177(8)	0.2189(8)
$y_{Sn/Ge}$	0.187(1)	0.190(1)	0.184(2)	0.187(2)	0.189(1)	0.190(1)
R_{Bragg} (%)	5.73	9.24	7.70	7.85	8.21	6.49
R_F (%)	5.04	7.88	6.11	6.71	7.62	5.02

field of 50 kOe is equal to 0.75 μ_B per Pr atom and is much smaller than the respective free Pr^{3+} ion value (3.2 μ_B).

Neutron diffraction patterns of $Pr_3Ag_4Sn_4$ recorded at low temperatures reveal the presence of additional peaks of magnetic origin. The patterns collected at 1.5, 9.5 and 20 K are shown in figure 2. Analysis indicates that the Pr magnetic moments occupy two sites with the following positions in the crystal unit cell:

- the 4e sites, $\mathbf{M}_1$ $(x, 0, 0)$, $\mathbf{M}_2$ $(1-x, 0, 0)$, $\mathbf{M}_3$ $(\frac{1}{2}+x, \frac{1}{2}, \frac{1}{2})$, $\mathbf{M}_4$ $(\frac{1}{2}-x, \frac{1}{2}, \frac{1}{2})$;
- the 2d sites, $\mathbf{M}_5$ $(\frac{1}{2}, 0, \frac{1}{2})$, $\mathbf{M}_6$ $(0, \frac{1}{2}, 0)$.

The analysis of the magnetic peak intensities leads to the following conclusions.

- At 1.5 K the Pr magnetic moments form a collinear order (propagation vector $\mathbf{k}_1 = (1, 1, 1)$) along the a-axis within both sublattices, with the magnetic moment values of 3.2(1) and 2.83(6) μ_B, and with the antiferromagnetic $-+$ and $++--$ moment sequences

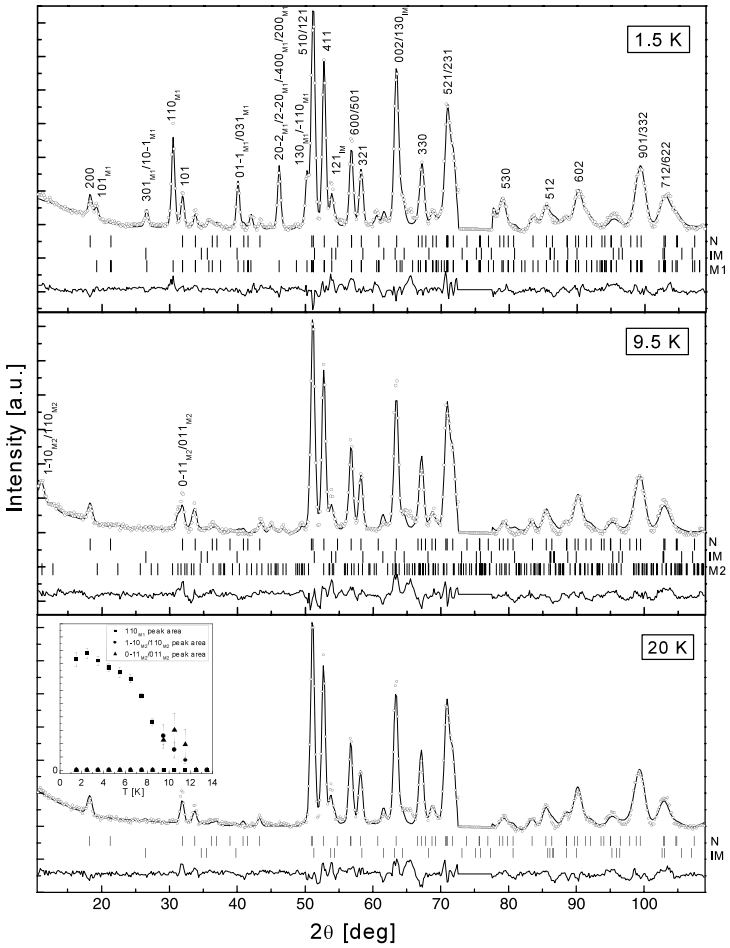

Figure 2. Neutron diffraction patterns of $Pr_3Ag_4Sn_4$ collected at 1.5, 9.5 and 20 K. The circles represent the experimental points; the solid curves are the calculated profiles for the model crystal and magnetic structures described in the text and the differences between the observed and calculated intensities (at the bottom of each diagram). The vertical bars indicate the Bragg peaks of nuclear (N for $Pr_3Ag_4Sn_4$ and IM for the $PrAg_2$ impurity phase) and magnetic (M1 and M2 for the phase connected with the $\mathbf{k}_1$ and $\mathbf{k}_2$ vectors, respectively) origin. The region around about 76° was excluded due to cryostat reflection. The inset shows the temperature dependence of the magnetic peak intensities.

for the 2d and 4e sublattices, respectively. Symmetry analysis supported by the MODY programme [11], carried out analogously to our previous works [1, 2], allows three irreducible representations (each of them appearing once) for the 2d sublattice and six irreducible representations (each of them appearing once as well) for the 4e sublattice (see tables 2 and 3) for the propagation vector $\mathbf{k} = (1, 1, 1)$. The fitted model is described by the τ_3 irreducible representation in both cases. $R_{\mathrm{mag1}} = 11.3\%$.

- At 9 K the magnetic moments of 2.8(4) μ_B in the 2d sublattice and of 2.4(2) μ_B in the 4e sublattice form the same arrangement as at lower temperatures, but the propagation vector becomes $\mathbf{k}_2 = (0, \frac{2}{3}, 0)$. The symmetry analysis allows three irreducible representations (each of them appearing once) for the 2d sublattice and four irreducible representations

Table 2. Basic vectors of the irreducible representations for $\mathbf{k} = (1, 1, 1)$ of the $Immm$ space group in the 2d positions.

	$(\frac{1}{2}, 0, \frac{1}{2})$	$(0, \frac{1}{2}, 0)$
τ_3	(1, 0, 0)	(−1, 0, 0)
τ_5	(0, 1, 0)	(0, −1, 0)
τ_7	(0, 0, 1)	(0, 0, −1)

Table 3. Basic vectors of the irreducible representations for $\mathbf{k} = (1, 1, 1)$ of the $Immm$ space group in the 4e positions.

	$(x, 0, 0)$	$(1 - x, 0, 0)$	$(\frac{1}{2} + x, \frac{1}{2}, \frac{1}{2})$	$(\frac{1}{2} - x, \frac{1}{2}, \frac{1}{2})$
τ_2	(1, 0, 0)	(−1, 0, 0)	(−1, 0, 0)	(1, 0, 0)
τ_3	(1, 0, 0)	(1, 0, 0)	(−1, 0, 0)	(−1, 0, 0)
τ_5	(0, 1, 0)	(0, 1, 0)	(0, −1, 0)	(0, −1, 0)
τ_6	(0, 0, 1)	(0, 0, −1)	(0, 0, −1)	(0, 0, 1)
τ_7	(0, 0, 1)	(0, 0, 1)	(0, 0, −1)	(0, 0, −1)
τ_8	(0, 1, 0)	(0, −1, 0)	(0, −1, 0)	(0, 1, 0)

Table 4. Basic vectors of the irreducible representations for $\mathbf{k} = (0, \frac{2}{3}, 0)$ of the $Immm$ space group in the 2d positions; $\varphi = \frac{2}{3}\pi$.

	$(\frac{1}{2}, 0, \frac{1}{2})$	$(0, \frac{1}{2}, 0)$
k		
τ_2	(0, 1, 0)	$(0, e^{i\varphi}, 0)$
τ_3	(1, 0, 0)	$(e^{i\varphi}, 0, 0)$
τ_4	(0, 0, 1)	$(0, 0, e^{i\varphi})$
−k		
τ_2	(0, −1, 0)	$(0, -e^{-i\varphi}, 0)$
τ_3	(1, 0, 0)	$(e^{-i\varphi}, 0, 0)$
τ_4	(0, 0, −1)	$(0, 0, -e^{-i\varphi})$

(two of them appearing twice) for the 4e sublattice (see tables 4 and 5) for the propagation vector $\mathbf{k} = (0, \frac{2}{3}, 0)$. The fitted model is described by the τ_3 irreducible representations in both cases. $R_{mag2} = 13.9\%$.

- At 12 K the magnetic moments disorder.

The temperature dependence of the magnetic 110_{M1}, $1–10_{M2}/110_{M2}$ and $0–11_{M2}/011_{M2}$ peak intensities shown in the inset in the figure 2 allows us to estimate the transition temperatures as equal to 9 and 12 K, the latter being the Néel temperature value. This result is consistent with the magnetic susceptibility measurement result.

3.2.2. $Nd_3Ag_4Sn_4$. Figure 3(a) shows the temperature dependence of the magnetic susceptibility and of the reciprocal magnetic susceptibility of $Nd_3Ag_4Sn_4$. In this case the temperature dependence of the magnetic susceptibility indicates a broad maximum about 4 K. Above the Néel temperature the reciprocal magnetic susceptibility satisfies the Curie–Weiss law, with a paramagnetic Curie temperature of −20.7 K and an effective Nd magnetic moment equal to 4.23 μ_B. The magnetization measured at 2 K in fields up to 50 kOe (see figure 3(b)) increases nearly linearly with increasing magnetic field; at 50 kOe it is equal to 0.75 μ_B per Nd atom and is much smaller than the respective free Nd^{3+} ion value (3.27 μ_B).

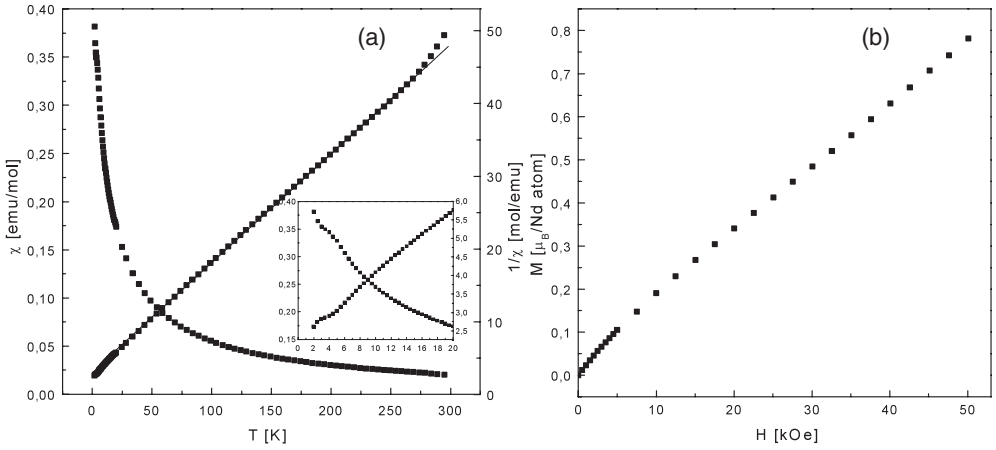

Figure 3. Temperature dependence of the magnetic susceptibility χ and the reciprocal magnetic susceptibility $1/\chi$ of $Nd_3Ag_4Sn_4$, measured at 1 kOe, and magnified 0–20 K region (part (a)) and magnetization curve measured at 2 K (part (b)).

Table 5. Basic vectors of the irreducible representations for $\mathbf{k} = (0, \frac{2}{3}, 0)$ of the *Immm* space group in the 4e positions; $\varphi = \frac{2}{3}\pi$.

	$(x, 0, 0)$	$(1-x, 0, 0)$	$(\frac{1}{2}+x, \frac{1}{2}, \frac{1}{2})$	$(\frac{1}{2}-x, \frac{1}{2}, \frac{1}{2})$
k				
τ_1	$(0, 0, 1)$	$(0, 0, -1)$	$(0, 0, e^{i\varphi})$	$(0, 0, -e^{i\varphi})$
τ_2	$(1, 0, 0)$	$(-1, 0, 0)$	$(e^{i\varphi}, 0, 0)$	$(-e^{i\varphi}, 0, 0)$
τ_2'	$(0, 1, 0)$	$(0, 1, 0)$	$(0, e^{i\varphi}, 0)$	$(0, e^{i\varphi}, 0)$
τ_3	$(1, 0, 0)$	$(1, 0, 0)$	$(e^{i\varphi}, 0, 0)$	$(e^{i\varphi}, 0, 0)$
τ_3'	$(0, 1, 0)$	$(0, -1, 0)$	$(0, e^{i\varphi}, 0)$	$(0, -e^{i\varphi}, 0)$
τ_4	$(0, 0, 1)$	$(0, 0, 1)$	$(0, 0, e^{i\varphi})$	$(0, 0, e^{i\varphi})$
$-\mathbf{k}$				
τ_1	$(0, 0, -1)$	$(0, 0, 1)$	$(0, 0, -e^{-i\varphi})$	$(0, 0, e^{-i\varphi})$
τ_2	$(1, 0, 0)$	$(-1, 0, 0)$	$(e^{-i\varphi}, 0, 0)$	$(-e^{-i\varphi}, 0, 0)$
τ_2'	$(0, -1, 0)$	$(0, -1, 0)$	$(0, -e^{-i\varphi}, 0)$	$(0, -e^{-i\varphi}, 0)$
τ_3	$(1, 0, 0)$	$(1, 0, 0)$	$(e^{-i\varphi}, 0, 0)$	$(e^{-i\varphi}, 0, 0)$
τ_3'	$(0, -1, 0)$	$(0, 1, 0)$	$(0, -e^{-i\varphi}, 0)$	$(0, e^{-i\varphi}, 0)$
τ_4	$(0, 0, -1)$	$(0, 0, -1)$	$(0, 0, -e^{-i\varphi})$	$(0, 0, -e^{-i\varphi})$

Neutron diffraction patterns of $Nd_3Ag_4Sn_4$ recorded at 1.5 and 10 K are shown in figure 4. The analysis of magnetic peak intensities leads to the following conclusions.

- At 1.5 K the Nd magnetic moments form a collinear order (propagation vector $\mathbf{k} = (1, 1, 1)$) with the magnetic moments of 1.3(1) μ_B parallel to the a-axis in the 2d sublattice and of 2.29(8) μ_B aligned in the a–b plane and forming an angle of 144(2)° on the a-axis for the 4e sublattice. The sequences of signs in the 2d and 4e sublattices are $+-$ and $++--$, respectively. Such order is described by the τ_3 irreducible representation in the case of the 2d sublattice and by linear combination of the the τ_3 and τ_5 irreducible representations in the case of the 4e sublattice (see tables 2 and 3). $R_{mag} = 19.4\%$.
- At 5 K the magnetic moments disorder.

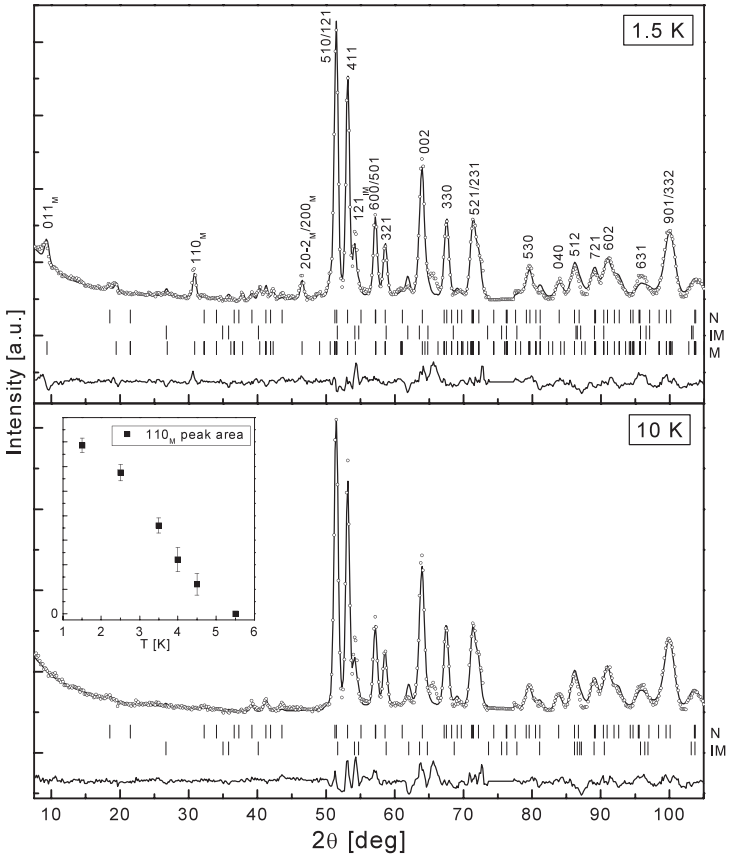

Figure 4. Neutron diffraction patterns of $Nd_3Ag_4Sn_4$ collected at 1.5 and 10 K. The circles represent the experimental points, the solid curves are the calculated profiles for the model crystal and magnetic structures described in the text and the differences between the observed and calculated intensities (at the bottom of each diagram). The vertical bars indicate the Bragg peaks of nuclear (N for $Nd_3Ag_4Sn_4$ and IM for the $NdAg_2$ impurity phase) and magnetic (M) origin. The region around about 76° was excluded due to cryostat reflection. The inset shows the temperature dependence of the magnetic 110_M peak intensity.

The temperature dependence of the magnetic 110_M peak intensity shown in the inset in the figure 4 allows us to estimate the Néel temperature value as equal to 5 K, which slightly surpasses the value obtained from the magnetic susceptibility data.

3.2.3. $Nd_3Cu_4Ge_4$. Figure 5(a) shows the temperature dependence of the magnetic susceptibility and of the reciprocal magnetic susceptibility of $Nd_3Cu_4Ge_4$. This dependence gives the Néel temperature value of 4 K, above which the reciprocal magnetic susceptibility satisfies the Curie–Weiss law with a paramagnetic Curie temperature of −4.0 K and an effective Nd magnetic moment equal to 3.64 μ_B. The magnetization measured at 2 K in fields up to 50 kOe (see figure 5(b)) increases nearly linearly with increasing magnetic field; at 50 kOe it is equal to 1.2 μ_B per Nd atom and is much smaller than the respective free Nd^{3+} ion value (3.27 μ_B).

Neutron diffraction patterns of $Nd_3Cu_4Ge_4$ recorded at 1.5 and 10 K are shown in figure 6. The analysis of magnetic peak intensities leads to the following conclusions.

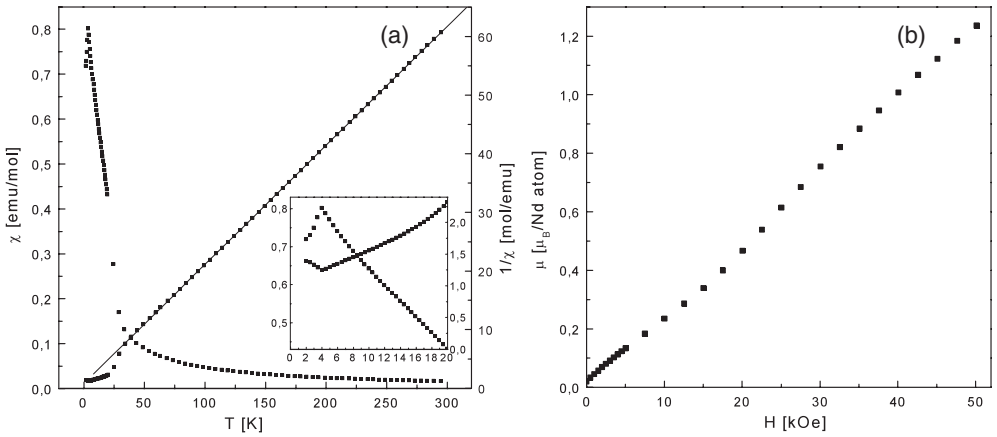

Figure 5. Temperature dependence of the magnetic susceptibility χ and the reciprocal magnetic susceptibility $1/\chi$ of $Nd_3Cu_4Ge_4$, measured at 1 kOe, and magnified 0–20 K region (part (a)) and magnetization curve measured at 2 K (part (b)).

- At 1.5 K the Nd magnetic moments are ordered only in the 4e sublattice forming a collinear structure (propagation vector $\mathbf{k} = (1, 1, 1)$) with the magnetic moments of 1.75(5) μ_B parallel to the c-axis with the $++--$ sequence of signs. Such order is described by the τ_7 irreducible representation (see table 3). $R_{mag} = 24.9\%$.
- At 4.5 K the magnetic moments disorder.

The temperature dependence of the magnetic 011_M peak intensity shown in the inset in figure 6 allows us to estimate the Néel temperature value as equal to 4.5 K, which slightly surpasses the value obtained from the magnetic susceptibility data.

4. Discussion

The investigated $R_3Ag_4Sn_4$ (R = Pr, Nd) and $Nd_3Cu_4Ge_4$ compounds crystallize in the orthorhombic $Gd_3Cu_4Ge_4$-type structure, in which the rare earth ions occupy two crystallographically inequivalent 2d and 4e sublattices. These compounds order antiferromagnetically at low temperatures forming different collinear structures. In the case of $Pr_3Ag_4Sn_4$, additional phase transition from collinear to non-collinear arrangement is observed. The low temperature magnetic structure of $Pr_3Ag_4Sn_4$ is the same as those of the isostructural $Pr_3Cu_4Sn_4$ [7] and $Ce_3Cu_4Sn_4$ [12]. For $Pr_3Cu_4Sn_4$ this structure is stable up to the Néel temperature while for $Ce_3Cu_4Sn_4$, similarly to the $Pr_3Ag_4Sn_4$ case, the collinear magnetic order changes to the modulated one near the Néel temperature. In all cases of the investigated compounds magnetic moment values of rare earth ions at 1.5 K are significantly reduced in comparison to the free R^{3+} ion values and they are different at different sites. It is likely that the reduction is caused by both the crystal electric field and the hybridization effect. A similar effect of the reduction of the light rare earth magnetic moments was observed in previous works [7, 12]. The determined Néel temperature values for the $R_3Ag_4Sn_4$ series—9 K for $Ce_3Ag_4Sn_4$ [13], 12 K for $Pr_3Ag_4Sn_4$ and 5 K for $Nd_3Ag_4Sn_4$—are larger than those resulting from de Gennes scaling based on the RKKY model [14] (see figure 7(a)). Also for the $R_3Cu_4Ge_4$ compounds the Néel temperature values are larger than those resulting from de Gennes scaling normalized to the Néel temperature of $Gd_3Cu_4Ge_4$ (8.6 K [15]) (see figure 7(b)). For light rare earths (R = Ce, Nd) the values of $\Delta T_N = T_N(\text{observed}) - T_N(\text{calculated})$

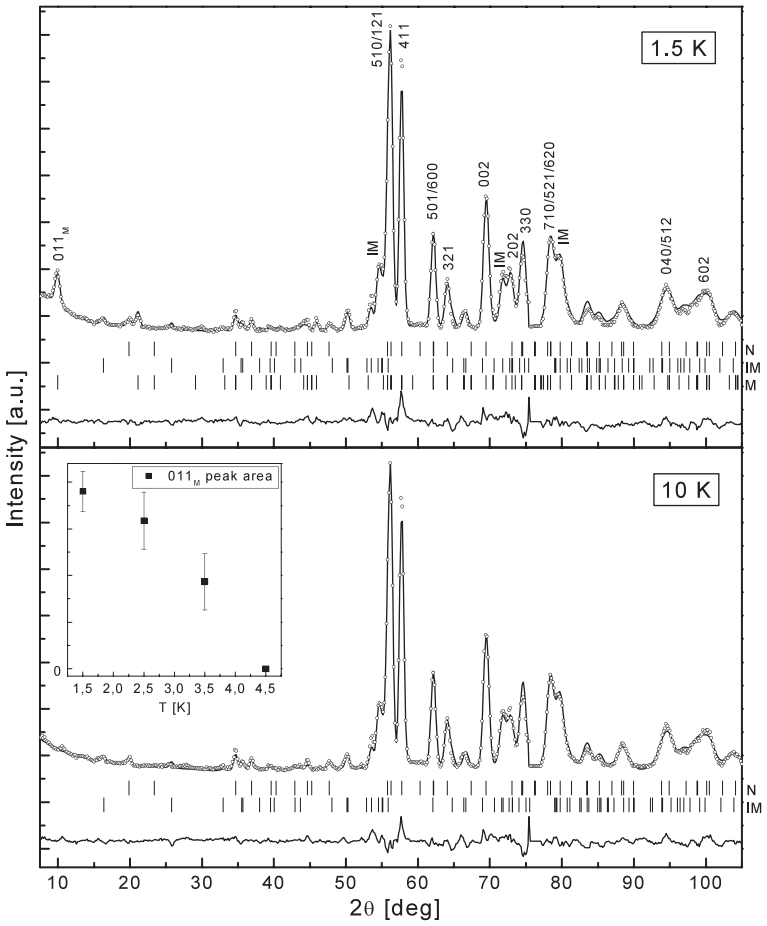

Figure 6. Neutron diffraction patterns of $Nd_3Cu_4Ge_4$ collected at 1.5 and 10 K. The circles represent the experimental points, the solid curves are the calculated profiles for the model crystal and magnetic structures described in the text and the differences between the observed and calculated intensities (at the bottom of each diagram). The vertical bars indicate the Bragg peaks of nuclear (N for $Nd_3Cu_4Ge_4$ and IM for the mix of the NdCuGe and $NdCuGe_2$ impurity phases) and magnetic (M) origin. The region around about 76° was excluded due to cryostat reflection. The inset shows the temperature dependence of the magnetic 011_M peak intensity.

decrease with increasing number of the 4f electrons. The difference between the observed and calculated Néel temperature values results from the strong influence of the crystalline electric field effect on the magnetic ordering schemes [16].

5. Conclusions

Results presented in this work as well as the previously obtained data [2, 7, 12] indicate complex magnetic ordering in the $R_3T_4X_4$, where R is a light rare earth element, compounds. This suggests that the main interaction leading to magnetic ordering in these systems is not purely of the RKKY type but is modified by the crystal electric field and/or hybridization effect. Investigations of the influence of this factor are planned.

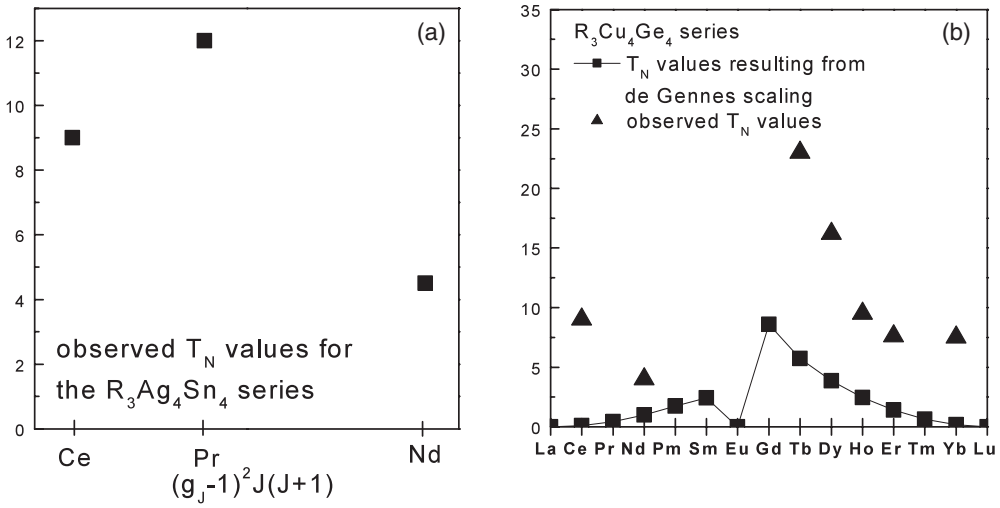

Figure 7. Observed Néel temperature values for the $R_3Ag_4Sn_4$ series (part (a)) and the Néel temperature values resulting from de Gennes scaling and observed Néel temperature values for the $R_3Cu_4Ge_4$ series (part (b)) [5, 15].

Acknowledgments

This research project has been supported by the European Commission under the Sixth Framework Programme through the Key Action 'Strengthening the European Research Area, research infrastructures', contract no HII3-CT-2003-505925 (NMI3), and by the State Committee for Scientific Research in Poland within the confines of grant 2P03B 113 23. The authors (EW and BP) would like to express their gratitude to the management of the Berlin Neutron Scattering Centre for their financial support and kind hospitality. Professor W Sikora from the University of Science and Technology in Cracow, Poland, is kindly acknowledged for permitting the authors to use the MODY programme.

References

[1] Wawrzyńska E, Hernández-Velasco J, Penc B, Sikora W, Szytuła A and Zygmunt A 2003 *J. Phys.: Condens. Matter* **15** 5279
[2] Wawrzyńska E, Baran S, Leciejewicz J, Sikora W, Stüßer N and Szytuła A 2003 *J. Phys.: Condens. Matter* **15** 803
[3] Szytuła A, Wawrzyńska E, Penc B, Stüßer N and Zygmunt A 2003 *Physica* B **327** 167
[4] Wawrzyńska E, Penc B, Stüßer N, Szytuła A and Tomkowicz Z 2003 *Solid State Commun.* **126** 527
[5] Wawrzyńska E, Hernández-Velasco J, Penc B, Szytuła A and Zygmunt A 2003 *J. Magn. Magn. Mater.* **264** 191
[6] Szytuła A, Wawrzyńska E, Penc B, Stüßer N, Tomkowicz Z and Zygmunt A 2004 *J. Alloys Compounds* **367** 224
[7] Wawrzyńska E, Hernández-Velasco J, Penc B and Szytuła A 2004 *J. Phys.: Condens. Matter* **16** 45
[8] Wawrzyńska E, Penc B, Hernández-Velasco J, Szytuła A and Zygmunt A 2003 *J. Alloys Compounds* **350** 68
[9] Rieger W 1970 *Mon. Chem.* **101** 449
[10] Rodriguez-Carvajal J 1993 *Physica* B **192** 55
[11] Sikora W, Pytlik L and Białas F 2003 *Neutron Scattering and Complementary Methods in Investigations of Condensed Phase* vol 1 (Poland: University of Podlasie Publishing House) p 55
[12] Zaharko O, Keller L and Ritter C 2002 *J. Magn. Magn. Mater.* **253** 130
[13] Boucelet P, Mazzone D, Noël H, Riani P, Rogl P and Ferro R 1999 *Intermetallics* **7** 931
[14] de Gennes P G 1962 *J. Phys. Radium* **23** 510
[15] Dhar S K, Singh S, Bonville P, Mazumdar C, Manfrinetti P and Palenzona A 2002 *Physica* B **312/313** 846
[16] Noakes D R and Shenoy G H 1982 *Phys. Lett.* A **91** 35